DiMonte, A.A., Ault, A.K., Hirth, G., and Bradbury, K.K., 2022, Hematite accommodated shallow, transient Pleistocene slow slip in the exhumed southern San Andreas fault system, California, USA: Geology, https://doi.org/10.1130/G50489.1

Geology – Supplemental Material

Hematite accommodated shallow, transient Pleistocene slow slip events in the exhumed southern San Andreas fault system, California, USA

Alexandra A. DiMonte[1], Alexis K. Ault[1], Greg Hirth[2], Kelly K. Bradbury[1]

[1]Department of Geosciences, Utah State University, Logan, UT 84322, USA
[2]Department of Earth, Environmental and Planetary Sciences, Providence, RI 02912, USA

1. Scanning electron microscopy and grain size analysis

Secondary electron (SE) and back-scattered electron (BSE) images, as well as energy dispersive spectroscopy (EDS) maps were acquired using a FEI Quanta FEG 650 field-emission scanning electron microscope (SEM) equipped with an Oxford EDS X-Max detector at Utah State University's Microscopy Core Facility. Hematite aliquots from samples listed in table S1 were affixed onto 1/2" and 1" metal posts with double-sided Cu adhesive tape in plan (slip surface) view and in cross-section (Fig. S8). C-coated 1" ring epoxy mounts were prepared from cm-scale slip surface cross-sections of samples D20-3a, D20-3b, D20-3c, D20-3d, D20-4a/i, D20-4b/ii, D20-6a, D20-8a, and D20-8b (Fig. S4).

C-coated mounts were analyzed under high vacuum at pressures of <5 x 10^{-6} torr with 10-20 kV accelerating voltage, and ~9-12 mm working distance. Cu adhesive tape mounts were imaged in low vacuum mode at pressures of 0.08-0.53 torr, with an accelerating voltage of 10-20 kV, and ~9-12 mm working distance. Images were acquired at ~100-250,000x magnification.

Hematite plate-width measurements (n = 1567) were conducted using the xT Microscope Control software on images acquired at 75,000-125,000x magnifying power. The hematite He closure temperature (T_c) was calculated for each measurement assuming Farley (2018) diffusion kinetics (E_a = 171 kJ/mol and $\ln(D_0)$ = -0.66), a spherical geometric factor, a cooling rate of 10 °C/Myr, and that the hematite plate half-width corresponds to the diffusion domain. Assuming an infinite plane sheet geometry increases the T_c values. Figure S7 presents histograms of hematite plate half-widths and calculated T_c.

2. Hematite (U-Th)/He analytical methods

Hematite aliquots were selected for (U-Th)/He analysis at the Utah State University's Mineral Microscopy and Spectroscopy Lab. Sub-mm aliquots were isolated from slip surfaces using fine-point tweezers under a stereomicroscope. Aliquots were pre-screened using SEM (see above) prior to (U-Th)/He analysis to identify and analyze aliquots comprising solely hematite, and thus exclude aliquots containing interstitial phases (i.e., calcite, quartz, chlorite). Because SEM-prescreening yield exterior views of three-dimensional aliquots, some dated aliquots may contain minor amounts of these interstitial phases.

Pre-screened aliquots were analyzed for He, U, and Th contents at the Arizona Radiogenic Helium Dating Laboratory at the University of Arizona in two sessions (November 2020 and May 2021). We used analytical methods described in Reiners et al. (2014), with some differences owing to the nature of our aliquots. Aliquots were heated with a diode laser in an ultra-high vacuum gas extraction line. This line has been modified to include a charcoal-filled, cold finger submerged in liquid N to scavenge reactive gases from laser-heated aliquots *in vacuo* prior to spike addition. Owing to the ultra-fine grain size, packets were lased at temperatures of ~850-900 °C, associated with a packet "very low glow" for 5 minutes. For most samples, a 3-minute gas re-extract was performed on the first aliquot per sample to confirm that measured $^{4}He/^{3}He$ ratios were at blank levels. Extracted He gas was spiked with ^{3}He, purified using cryogenic and gettering methods, and analyzed and measured on a quadrupole mass spectrometer. Analysis of a known quantity of ^{4}He was performed after every ~8 unknown analyses to monitor instrumental sensitivity drift. Each planchette of Fe-oxides is processed with several line blanks and hot blanks (on empty Nb packets) to constrain the $^{4}He/^{3}He$ ratios of unknown aliquots, together with $^{4}He/^{3}He$ ratios of ^{3}He shots. ^{4}He blanks from these procedures are ~0.05 fmol.

U and Th contents of each aliquot were measured by isotope dilution and solution ICPMS following the methods detailed in (Reiners, 2005). The degassed packets were dissolved in hydrochloric acid in a pressure digestion vessel (Parr bomb). Following addition of a ^{233}U-^{229}Th spike, equilibration, and dissolution, U and Th isotopes were measured on an Element 2 ICP-MS. The ^{233}U-^{229}Th spike contains 0.4-0.8 ng of ^{233}U and 0.6-1.2 ng of ^{229}Th. Example $^{238}U/^{233}U$ values of spike blanks and spike normals that accompanied each ICP-MS run are 0.00357 ± 0.00007 (± 1σ) and 1.27864 ± 0.004323 (± 1σ), respectively. Example $^{232}Th/^{229}Th$ values spike blanks and spike normals are 0.001575 ± 0.000073 (± 1σ) and 2.306317 ± 0.016291 (± 1σ), respectively. Typical background corrections for U and Th come from analysis of the same empty Nb tubes and are 0.001 ± 0.0001 ng U (± 1σ) and 0.0005 ± 0.0001 ng Th (± 1σ).

Blank corrected (U-Th)/He dates were calculated with propagated analytical uncertainties from U, Th, and He measurements. Hematite dates were determined assuming that the grains were unzoned in U and Th. Dates in Table S2 are not reported with an F_t correction, assuming He implantation balances alpha (α)-ejection. Some samples with hematite slip surfaces have hematite preserved on both sides of the fault, and aliquots that were extracted from these surfaces are larger than the α-stopping distance.

3. F_T correction to hematite (U-Th)/He dates

Within a polycrystalline hematite aliquot, alpha ejection is assumed to balance implantation between individual crystals within the mass, so we consider He loss from the aliquot to its surroundings. We explore the possibility of α-ejection from hematite aliquots through one side or both sides of the targeted material (Fig. S9, S10; Table S3). Calculations assume a Th/U ratio of 0.045 (average of the entire dataset), a weighted α stopping distance of 13.605 μm for U^{238} and U^{235}, an α stopping distance of 16.04 μm for Th^{232} (Ketcham et al., 2011), a uniform distribution of U and Th, and an aliquot width of 75 μm (lower range of observed aliquot widths). Evaluation of the F_T correction was implemented in a Python code (DR#), which performs n =

10,000,000 calculations that converge on an (1) $F_t = 0.94$, for $\alpha-$ ejection from only one side of the aliquot and, (2) $F_t = 0.88$, for α ejection from both sides of the aliquot. F_T-corrected dates do not change the overall interpretation of the data patterns.

4. Discussion of hematite (U-Th)/He data outliers and secular disequilibrium

Aliquots analyzed for hematite (U-Th)/He thermochronometry are small volume, owing to efforts to target specific textures and pure hematite, and young. We report all analyses in Table S2, but do not discuss a subset (19%) of analyses in the main text with analytical issues. These manifest as (1) low U content, (2) anomalously high Th/U ratios, and (3) low He content. We discuss these data and issues here.

First, aliquots 3cii-B4, 3di-A2, 4i-D1, 4ii-B4, 6aii-E1, 8ai-E4, 8aii-E1, and 17h-B4 yield U content that is lower compared to other aliquots from the same sample. We set a cutoff of a z-score <-1.25 for inclusion in the main text discussion. Samples with anomalously low U may have lost U during degassing. Second, aliquot 8ai-D3 has an anomalously high Th/U ratio (7.583) compared to aliquots within the sample and across the entire dataset, and U may have been lost during degassing (Hofmann et al., 2020; Vasconcelos et al., 2013). In general, we observe no positive *intrasample* trends between hematite He date and Th/U that would reflect U loss (Fig. S11). Third, aliquot 18ci-A2 yields anomalously low He content both within the sample and across the dataset, suggesting that He extraction during degassing was incomplete. In addition, we do not discuss aliquot 8ai-C6 because it was the only aliquot without analytical issues for sample 8ai. To do so would place significance on an individual analysis, which is not standard practice in (U-Th)/He thermochronometry. Finally, the (U-Th)/He date for 8aii-C2 is not discussed because it a notable outlier for the sample, but the cause of analytical dispersion is unknown.

Secular disequilibrium due to chemical fractionation within the ^{238}U decay series impacts the He ingrowth rate in minerals with crystallization ages <1 Ma. [$^{234}U/^{238}U$] and [$^{230}Th/^{238}U$] activity ratios that are >1 and <1 cause (U-Th)/He dates to be older than or younger than the “true age,” respectively, provided dates record formation and not cooling. Although we lack [$^{234}U/^{238}U$] and [$^{230}Th/^{238}U$] activity ratios for our dataset, it is likely that, for aliquots with (U-Th)/He dates >400 ka, low Th/U, and low U concentration, the error associated with our individual analyses is <±15% (Farley et al., 2002). This error overlaps in part with calculated sample standard deviations from dates that record formation ages, which range from 4-15% (Table S1). Consideration of the worst-case scenario does not influence the overall interpretation of our hematite He dates as mineralization dates. Because analytical error due to secular disequilibrium is larger with younger dates and exceeds the maximum percent standard deviation, we do not discuss three aliquots (26a-A1, 26bii-F3, and 20a-A1) in the main text with dates <<0.30 Ma.

References

Farley, K. A., 2018, Helium diffusion parameters of hematite from a single-diffusion-domain crystal: Geochimica et Cosmochimica Acta, v. 231, p. 117-129.

Hofmann, F., Treffkorn, J., and Farley, K. A., 2020, U-loss associated with laser-heating of hematite and goethite in vacuum during (U–Th)/He dating and prevention using high O2 partial pressure: Chemical Geology, v. 532, p. 119350.

Ketcham, R. A., Gautheron, C., and Tassan-Got, L., 2011, Accounting for long alpha-particle stopping distances in (U-Th-Sm)/He geochronology: refinement of the baseline case: Geochimica et Cosmochimica Acta, v. 75, p. 7779-7791.

Reiners, P. W., 2005, Zircon (U-Th)/He thermochronometry: Reviews in Mineralogy and Geochemistry, v. 58, p. 151-179.

Reiners, P. W., Chan, M. A., and Evenson, N. S., 2014, Radiogenic helium dating and chemistry of diagenetic Fe- and Mn-oxides in Mesozoic sandstones of the Colorado Plateau: Geological Society of America Bulletin, v. 126, no. 9-10, p. 1363-1383.

Vasconcelos, P. M., Heim, J. A., Farley, K. A., Monteiro, H., and Waltenberg, K., 2013, $^{40}Ar/^{39}Ar$ and (U-Th)/He - $^{4}He/^{3}He$ geochronology of landscape evolution and channel iron deposits genesis at Lynn Peak, Western Australia: Geochimica et Cosmochimica Acta, v. 117, p. 283-312.

Table S1. Sample information and locations with samples analyzed for (U-Th)/He hematite thermochronometry and included in main text highlighted.

Sample	*Type* [a]	*SEM ID*	*Hem He?*	*SEM?*	*Slip Surface*	*Slickenline*	*GPS Location*	*Elevation*
D20-1a	hematite ss				047/55	46-->181	33.63353, -115.99178	182 m
D20-2	basement						33.63087, -115.99118	301 m
D20-3a	hematite ss		x	x	102/85	curved	33.61606, -115.99806	177 m
D20-3b	hem/clay ss			x	129/66	30NW	33.61606, -115.99806	177 m
D20-3c	hematite ss		x	x	135/54	90SE (dip)	33.61606, -115.99806	177 m
D20-3d	hematite ss		x	x			33.61606, -115.99806	177 m
D20-3e	silica ss						33.61606, -115.99806	177 m
D20-4a		D20-4i	x	x				
D20-4b	hematite ss	D20-4ii	x	x	105/15, 205/56, 181/27, 151/66, 244/90	14-->205	33.61622, -115.99790	166 m
D20-4c		D20-4iii		x				
D20-5	hematite ss				143/27		33.61508, -115.99854	320 m
D20-6a	hematite ss		x	x	255/77	43SE	33.61684, -115.99954	181 m
D20-6b	hematite ss				285/38		33.61684, -115.99954	181 m
D20-6c	hematite ss						33.61684, -115.99954	181 m
D20-6d	hematite ss						33.61684, -115.99954	181 m
D20-6e	hematite ss						33.61684, -115.99954	181 m
D20-7	gouge				253/42, 224/46		33.61634, -115.99943	177 m
D20-8a	hematite ss		x	x	137/79		33.61498, -116.00181	127 m
D20-8b	hematite ss		x	x			33.61498, -116.00181	127 m
D20-9	paly ss							
D20-10a	hematite ss						33.61627, -115.99769	159 m
D20-10b	gouge						33.61627, -115.99769	159 m
D20-10c	clay				328/74, 324/71		33.61627, -115.99769	159 m
D20-10d	hem/clay ss				256/53		33.61627, -115.99769	159 m
D20-12a	hem ss						33.61639, -115.99781	178 m
D20-12b	hem/clay ss						33.61639, -115.99781	178 m
D20-12c	basement						33.61639, -115.99781	178 m
D20-13	hem/clay ss						33.61634, -115.99814	181 m
D20-14	clay						33.61605, -115.99803	168 m

Table S1 (continued).

Sample	*Type* [a]	*SEM ID*	*Hem He?*	*SEM?*	*Slip Surface*	*Slickenline*	*GPS Location*	*Elevation*
D20-15A	clay				290/87		33.61590, -115.99881	163 m
D20-15b	cat/gouge				308/78		33.61590, -115.99881	163 m
D20-16	hematite ss						33.61608, -115.99881	165 m
D20-17a-h	hematite ss		x	x	245/88		33.61627, -115.99848	177 m
D20-18a	breccia						33.61678, -115.9940	185 m
D20-18b	gouge						33.61678, -115.9940	185 m
D20-18c	hematite ss	D20-18ci	x	x			33.61678, -115.9940	185 m
D20-18d		D20-18cii	x	x				
D20-19a	hematite ss						33.61670, -116.00082	214 m
D20-19b	alt volc						33.61670, -116.00082	214 m
D20-20a	hematite ss		x	x			33.61957, -116.05000	315 m
D20-20b	breccia						33.61957, -116.05000	315 m
D20-22a	alt volc						33.61522, -116.00076	129 m
D20-22b	clay						33.61522, -116.00076	129 m
D20-22c	red clay				043/35	30-->133	33.61522, -116.00076	129 m
D20-22d	hematite ss						33.61522, -116.00076	129 m
D20-23a	gr/black surf				023/81, 001/84		33.61516, -116.00077	178 m
D20-23b	hem/chlor ss						33.61516, -116.00077	178 m
D20-23c	hem/chlor ss						33.61516, -116.00077	178 m
D20-24	hematite ss						33.61588, -116.00329	190 m
D20-25a	hematite ss				111/78, 092/63		33.62817, -115.98956	345 m
D20-25b	mix hem/clay						33.62817, -115.98956	345 m
D20-26a	hematite ss		x	x			33.62940, -115.98999	267 m
D20-26b	hematite ss	D20-26bii	x	x			33.62940, -115.98999	267 m

[a] ss = slip surfaces. basement = crystaline basement, hem = hematite, paly = palygorskite, cat = cataclasite, alt volc = altered crystalline rock, gr/black surf = joint surface with green-black mineral, chlor = chlorite

Table S2. Hematite (U-Th)/He thermochronometry data.

Sample	U (ng)	± 1σ	z U	Th (ng)	± 1σ	Th/U	He (fmol)	± 1σ	Date (Ma)	2σ (Ma)
D20-3a-A3	0.460	0.0067	-1.003	0.003	0.0001	0.007	1.551	0.051	0.63	0.04
D20-3a-B2	1.226	0.0175	1.016	0.005	0.0001	0.004	3.773	0.060	0.57	0.02
D20-3a-C2	1.346	0.0193	1.332	0.006	0.0001	0.004	4.198	0.057	0.58	0.02
D20-3a-D4	0.728	0.0104	-0.297	0.003	0.0001	0.004	2.489	0.048	0.63	0.03
D20-3a-D1	0.443	0.0064	-1.048	0.003	0.0001	0.007	1.631	0.049	0.68	0.05
								Mean	**0.62**	
								Std. Dev	**0.04**	**7%**
D20-3cii-A2	0.334	0.0049	0.484	0.022	0.0003	0.068	0.965	0.051	0.53	0.06
D20-3cii-B2	0.386	0.0080	1.053	0.034	0.0008	0.091	0.902	0.044	0.42	0.04
[a]D20-3cii-B4	0.167	0.0024	-1.344	0.004	0.0001	0.024	0.894	0.043	0.99	0.10
D20-3cii-C2	0.369	0.0053	0.861	0.007	0.0001	0.020	0.840	0.046	0.42	0.05
D20-3cii-D2	0.193	0.0028	-1.054	0.002	0.0001	0.012	0.628	0.041	0.60	0.08
								Mean	**0.49**	
								Std. Dev	**0.08**	**15%**
D20-3di-A1	0.464	0.0067	1.669	0.012	0.0002	0.026	1.828	0.051	0.73	0.04
D20-3di-A2	0.200	0.0029	-1.328	0.004	0.0001	0.021	0.618	0.047	0.57	0.09
D20-3di-B1	0.333	0.0048	0.174	0.004	0.0001	0.012	1.086	0.048	0.60	0.06
D20-3di-B5	0.328	0.0047	0.123	0.007	0.0001	0.021	1.215	0.052	0.68	0.06
D20-3di-C3	0.261	0.0038	-0.638	0.019	0.0003	0.075	0.825	0.044	0.58	0.06
D20-3dii-B1	0.632	0.0090	-0.276	0.011	0.0002	0.017	2.373	0.053	0.69	0.04
D20-3dii-C2	1.409	0.0202	1.688	0.007	0.0002	0.005	6.655	0.063	0.88	0.03
D20-3dii-E4	0.384	0.0057	-0.903	0.005	0.0001	0.013	1.373	0.022	0.66	0.03
D20-3dii-F1	0.539	0.0078	-0.510	0.005	0.0001	0.009	2.165	0.040	0.74	0.03
								Mean	**0.70**	
								Std. Dev	**0.09**	**12%**
D20-4a-C1	0.901	0.0130	1.320	0.009	0.0001	0.010	3.661	0.053	0.75	0.03
D20-4a-D1	0.233	0.0034	-1.478	0.004	0.0001	0.017	0.848	0.023	0.67	0.04
D20-4a-D5	0.646	0.0093	0.254	0.015	0.0003	0.024	2.339	0.040	0.67	0.03
D20-4a-D6	0.562	0.0081	-0.097	0.006	0.0001	0.010	2.160	0.041	0.71	0.03
								Mean	**0.71**	
								Std. Dev	**0.03**	**5%**
D20-4b-A5	0.405	0.0058	1.240	0.009	0.0002	0.024	1.477	0.038	0.67	0.04
D20-4b-B4	0.248	0.0036	-1.521	0.024	0.0004	0.101	1.358	0.031	0.99	0.05
D20-4b-B7	0.329	0.0047	-0.093	0.050	0.0007	0.154	1.123	0.033	0.61	0.04
D20-4b-C5	0.356	0.0052	0.374	0.012	0.0002	0.035	0.902	0.037	0.47	0.04
								Mean	**0.58**	
								Std. Dev	**0.09**	**15%**

Table S2 (continued).

Sample	U (ng)	± 1σ	z U	Th (ng)	± 1σ	Th/U	He (fmol)	± 1σ	Date (Ma)	2σ (Ma)
D20-6aii-B4	0.414	0.0059	0.339	0.046	0.0007	0.113	2.622	0.042	1.15	0.05
D20-6aii-C2	0.380	0.0055	0.110	0.041	0.0007	0.112	2.079	0.037	0.99	0.04
D20-6aii-C4	0.535	0.0078	1.149	0.082	0.0012	0.158	3.636	0.056	1.22	0.05
D20-6aii-E1	0.124	0.0018	-1.598	0.036	0.0006	0.303	0.771	0.034	1.08	0.10
D20-6aiii-C1	0.822	0.0118	1.528	0.025	0.0004	0.032	9.900	0.120	2.22	0.08
D20-6aiii-C4	0.291	0.0042	-1.055	0.016	0.0003	0.058	2.217	0.032	1.40	0.06
D20-6aiii-D1	0.556	0.0080	0.234	0.031	0.0004	0.057	4.159	0.058	1.37	0.05
D20-6aiii-D4	0.362	0.0052	-0.706	0.028	0.0005	0.079	2.938	0.047	1.48	0.06
								Mean	**1.40**	
								Std. Dev	**0.37**	**26%**
D20-8ai-C6	0.142	0.0021	0.088	0.009	0.0001	0.066	0.744	0.029	0.96	0.08
D20-8ai-D3	0.189	0.0028	1.178	1.398	0.0200	7.583	2.377	0.040	0.85	0.03
D20-8ai-E4	0.082	0.0012	-1.266	0.007	0.0002	0.082	0.611	0.027	1.35	0.13
D20-8aii-C2	0.365	0.0052	0.690	0.013	0.0002	0.038	0.620	0.026	0.31	0.03
D20-8aii-E1	0.273	0.0039	-1.612	0.004	0.0001	0.016	1.083	0.024	0.73	0.04
D20-8aii-E2	0.336	0.0049	-0.039	0.021	0.0003	0.065	1.464	0.034	0.80	0.04
D20-8aii-E4	0.375	0.0054	0.961	0.005	0.0001	0.014	1.603	0.043	0.79	0.05
								Mean	**0.79**	
								Std. Dev	**0.00**	**0.5%**
D20-8b-B4	0.651	0.0094	-0.528	0.061	0.0009	0.096	3.177	0.051	0.89	0.04
D20-8b-D5	0.919	0.0131	0.191	0.188	0.0027	0.210	3.603	0.060	0.69	0.03
D20-8b-F1	0.427	0.0061	-1.127	0.006	0.0001	0.015	1.539	0.039	0.67	0.04
D20-8b-C1	0.717	0.0103	-0.351	0.019	0.0003	0.027	2.430	0.047	0.63	0.03
D20-8b-C6	1.526	0.0221	1.815	0.049	0.0007	0.033	5.377	0.038	0.65	0.02
								Mean	**0.70**	
								Std. Dev	**0.09**	**13%**
D20-17g-B4	0.305	0.0045	1.299	0.005	0.0002	0.016	0.785	0.022	0.48	0.03
D20-17g-C4	0.194	0.0028	-0.166	0.004	0.0001	0.019	0.550	0.021	0.53	0.04
D20-17g-D2	0.120	0.0018	-1.133	0.002	0.0001	0.019	0.275	0.018	0.42	0.06
								Mean	**0.48**	
								Std. Dev	**0.04**	**9%**

Table S2 (continued).

Sample	U (ng)	± 1σ	z U	Th (ng)	± 1σ	Th/U	He (fmol)	± 1σ	Date (Ma)	2σ (Ma)
D20-17h-A3	0.815	0.0119	1.031	0.026	0.0004	0.033	2.404	0.029	0.54	0.02
D20-17h-B2	0.713	0.0104	0.552	0.011	0.0002	0.017	1.674	0.028	0.43	0.02
D20-17h-B3	0.683	0.0100	0.410	0.008	0.0002	0.012	1.878	0.019	0.51	0.02
D20-17h-B4	0.159	0.0024	-2.051	0.004	0.0001	0.025	0.396	0.016	0.46	0.04
D20-17h-C2	0.526	0.0078	-0.328	0.003	0.0001	0.005	1.481	0.020	0.52	0.02
D20-17h-C4	0.678	0.0099	0.386	0.008	0.0002	0.012	1.803	0.022	0.49	0.02
								Mean	**0.50**	
								Std. Dev	**0.04**	**7%**
D20-18c-A1	0.592	0.0086	-0.638	0.011	0.0002	0.019	1.987	0.025	0.62	0.02
D20-18c-A2	0.920	0.0136	0.759	0.013	0.0003	0.015	1.614	0.026	0.32	0.01
D20-18c-B1	0.517	0.0076	-0.956	0.056	0.0009	0.111	2.021	0.030	0.71	0.03
D20-18c-B2	0.564	0.0084	-0.756	0.030	0.0005	0.054	1.917	0.041	0.62	0.03
D20-18c-C3	1.116	0.0162	1.591	0.016	0.0003	0.015	3.640	0.040	0.60	0.02
								Mean	**0.64**	
								Std. Dev	**0.04**	**6%**
D20-18d-C4	0.515	0.0076	-1.026	0.011	0.0002	0.022	1.750	0.030	0.63	0.03
D20-18d-D4	0.826	0.0120	0.463	0.025	0.0004	0.031	3.008	0.044	0.67	0.03
D20-18d-Z1	1.025	0.0149	1.416	0.016	0.0003	0.016	2.901	0.048	0.52	0.02
D20-18d-Z2	0.551	0.0080	-0.853	0.008	0.0001	0.015	1.620	0.032	0.54	0.03
								Mean	**0.59**	
								Std. Dev	**0.06**	**10%**
D20-20a-A1	2.554	0.0438	1.902	0.094	0.0014	0.038	1.664	0.038	0.12	0.01
D20-20a-B4	0.686	0.0100	-1.017	0.008	0.0002	0.012	1.868	0.038	0.50	0.02
D20-20a-C3	1.303	0.0191	-0.054	0.016	0.0003	0.013	3.076	0.045	0.44	0.02
D20-20a-D2	1.067	0.0156	-0.422	0.014	0.0002	0.014	2.208	0.037	0.38	0.02
D20-20a-D4	1.075	0.0156	-0.409	0.135	0.0020	0.129	2.371	0.039	0.40	0.02
								Mean	**0.43**	
								Std. Dev	**0.05**	**11%**
D20-26a-A1	0.238	0.0035	-1.082	0.052	0.0008	0.225	0.317	0.008	0.23	0.01
D20-26a-B1	0.820	0.0119	-0.457	0.035	0.0006	0.044	1.474	0.020	0.33	0.01
D20-26a-B2	1.062	0.0154	-0.197	0.023	0.0005	0.022	2.711	0.037	0.47	0.02
D20-26a-C2	1.104	0.0159	-0.151	0.025	0.0004	0.023	2.663	0.032	0.45	0.02
D20-26a-D2	3.000	0.0173	1.887	0.059	0.0009	0.051	2.815	0.041	0.43	0.02
								Mean	**0.42**	
								Std. Dev	**0.05**	**13%**

Table S2 (continued).

Sample	U (ng)	± 1σ	z U	Th (ng)	± 1σ	Th/U	He (fmol)	± 1σ	Date (Ma)	2σ (Ma)
D20-26b-B4	0.651	0.0097	-0.320	0.007	0.0001	0.011	1.258	0.026	0.36	0.02
D20-26b-C3	2.527	0.0367	1.709	0.027	0.0004	0.011	4.723	0.024	0.35	0.01
D20-26b-E5	0.382	0.0057	-0.612	0.008	0.0001	0.021	0.793	0.012	0.38	0.02
D20-26b-F3	0.229	0.0033	-0.777	0.008	0.0002	0.036	0.315	0.013	0.25	0.02
								Mean	**0.36**	
								Std. Dev	**0.02**	**4%**

[a]Blue samples are outlier analyses that are not included in the geometric mean calculation. See text S4 for discussion of outlier analyses.

Table S3. F_T-corrected hematite (U-Th)/He dates. See text S3 for discussion.

Sample	Raw Date (Ma)	Ejected from one side (F_T = 0.94) Date (Ma)	Δ Date (Ma)[a]	Ejected from both sides (F_T = 0.88) Date (Ma)	Δ Date (Ma)[a]
D20-3a-A3	0.63	0.67	0.04	0.71	0.09
D20-3a-B2	0.57	0.61	0.04	0.65	0.08
D20-3a-C2	0.58	0.62	0.04	0.66	0.08
D20-3a-D4	0.63	0.68	0.04	0.72	0.09
D20-3a-D1	0.68	0.73	0.04	0.78	0.09
D20-3cii-A2	0.53	0.56	0.03	0.60	0.07
D20-3cii-B2	0.42	0.45	0.03	0.48	0.06
D20-3cii-C2	0.42	0.45	0.03	0.48	0.06
D20-3cii-D2	0.60	0.64	0.04	0.68	0.08
D20-3di-A1	0.73	0.77	0.05	0.83	0.10
D20-3di-B1	0.60	0.64	0.04	0.69	0.08
D20-3di-B5	0.68	0.73	0.04	0.78	0.09
D20-3di-C3	0.58	0.61	0.04	0.66	0.08
D20-3dii-B1	0.69	0.74	0.04	0.79	0.09
D20-3dii-C2	0.88	0.93	0.06	1.00	0.12
D20-3dii-E4	0.66	0.70	0.04	0.75	0.09
D20-3dii-F1	0.74	0.79	0.05	0.85	0.10
D20-4a-C1	0.75	0.80	0.05	0.86	0.10
D20-4a-D5	0.67	0.71	0.04	0.76	0.09
D20-4a-D6	0.71	0.76	0.05	0.81	0.10
D20-4b-A5	0.67	0.72	0.04	0.77	0.09
D20-4b-B7	0.61	0.65	0.04	0.70	0.08
D20-4b-C5	0.47	0.50	0.03	0.53	0.06
D20-6aii-B4	1.15	1.22	0.07	1.30	0.16
D20-6aii-C2	0.99	1.05	0.06	1.13	0.14
D20-6aii-C4	1.22	1.29	0.08	1.38	0.17
D20-6aiii-C1	2.22	2.36	0.14	2.52	0.30
D20-6aiii-C4	1.40	1.49	0.09	1.59	0.19
D20-6aiii-D1	1.37	1.46	0.09	1.56	0.19
D20-6aiii-D4	1.48	1.57	0.09	1.68	0.20
D20-8aii-E2	0.80	0.85	0.05	0.91	0.11
D20-8aii-E4	0.79	0.84	0.05	0.90	0.11

Table S3 (continued).

Sample	Raw Date (Ma)	Ejected from one side (F_T = 0.94) Date (Ma)	Δ Date (Ma)[a]	Ejected from both sides (F_T = 0.88) Date (Ma)	Δ Date (Ma)[a]
D20-8b-B4	0.89	0.94	0.06	1.01	0.12
D20-8b-D5	0.69	0.74	0.04	0.79	0.09
D20-8b-F1	0.67	0.71	0.04	0.76	0.09
D20-8b-C1	0.63	0.67	0.04	0.71	0.09
D20-8b-C6	0.65	0.69	0.04	0.74	0.09
D20-20a-B4	0.50	0.54	0.03	0.57	0.07
D20-20a-C3	0.44	0.47	0.03	0.50	0.06
D20-20a-D2	0.38	0.41	0.02	0.44	0.05
D20-20a-D4	0.40	0.42	0.03	0.45	0.05
D20-17g-B4	0.48	0.51	0.03	0.54	0.06
D20-17g-C4	0.53	0.56	0.03	0.60	0.07
D20-17g-D2	0.42	0.45	0.03	0.48	0.06
D20-17h-A3	0.54	0.58	0.03	0.62	0.07
D20-17h-B2	0.43	0.46	0.03	0.49	0.06
D20-17h-B3	0.51	0.54	0.03	0.58	0.07
D20-17h-C2	0.52	0.56	0.03	0.59	0.07
D20-17h-C4	0.49	0.52	0.03	0.56	0.07
D20-18c-A1	0.62	0.66	0.04	0.71	0.08
D20-18c-B1	0.71	0.75	0.05	0.80	0.10
D20-18c-B2	0.62	0.66	0.04	0.71	0.09
D20-18c-C3	0.60	0.64	0.04	0.69	0.08
D20-18d-C4	0.63	0.67	0.04	0.71	0.09
D20-18d-D4	0.67	0.71	0.04	0.76	0.09
D20-18d-Z1	0.52	0.56	0.03	0.60	0.07
D20-18d-Z2	0.54	0.58	0.03	0.62	0.07
D20-26a-B1	0.33	0.35	0.02	0.38	0.05
D20-26a-B2	0.47	0.50	0.03	0.54	0.06
D20-26a-C2	0.45	0.47	0.03	0.51	0.06
D20-26a-D2	0.43	0.46	0.03	0.49	0.06
D20-26b-B4	0.36	0.38	0.02	0.41	0.05
D20-26b-C3	0.35	0.37	0.02	0.39	0.05
D20-26b-E5	0.38	0.41	0.02	0.44	0.05

[a]Δ = increase in date (Ma) after applying F_T correction

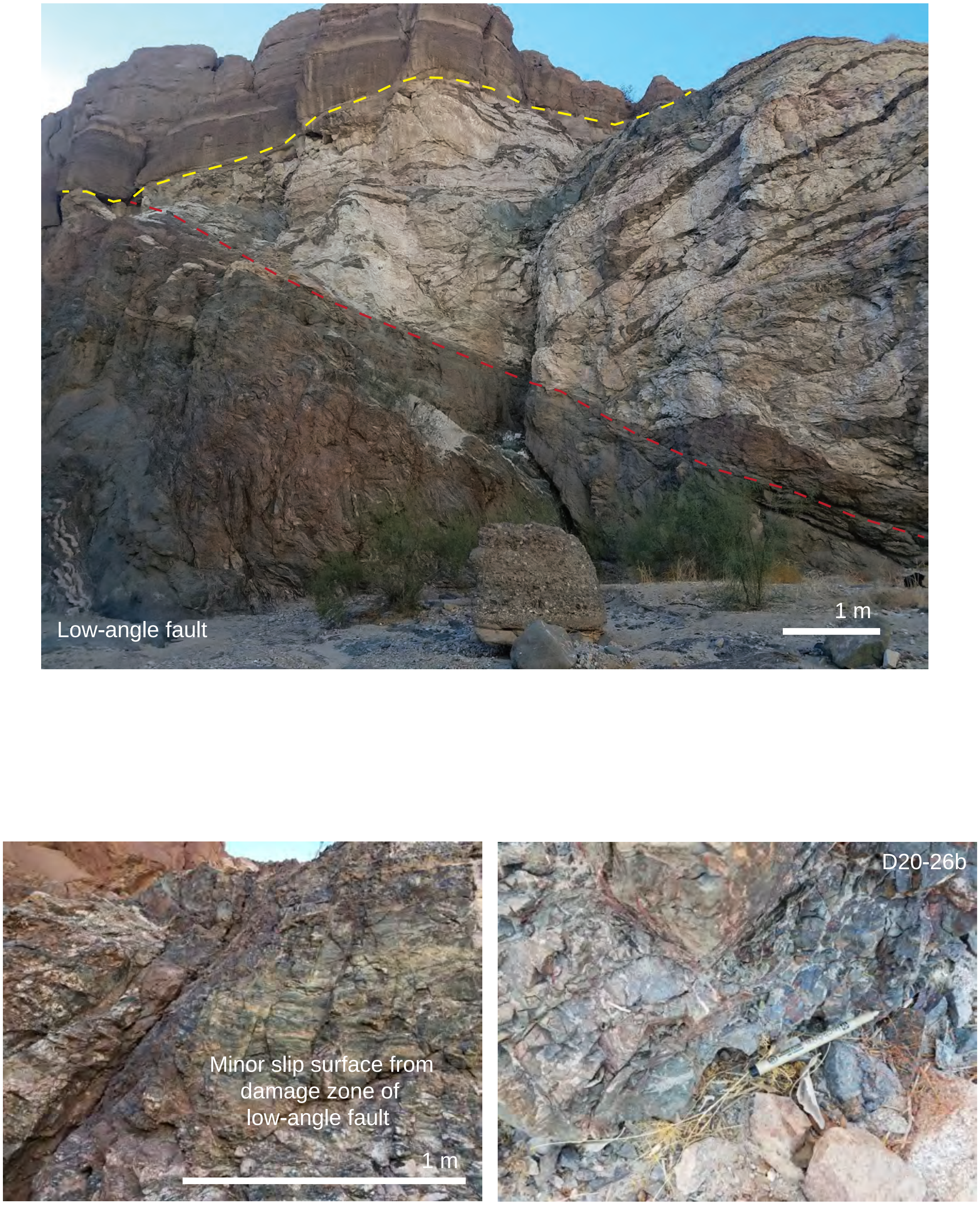

Figure S1. Map-scale low-angle fault cutting basement rock in Platform block. Dashed red line = fault surface. Dashed yellow line = basement-Pleistocene sediment nonconformity. Associated damage zone structures including minor fault (lower left) and hematite-coated slip surface (lower right.)

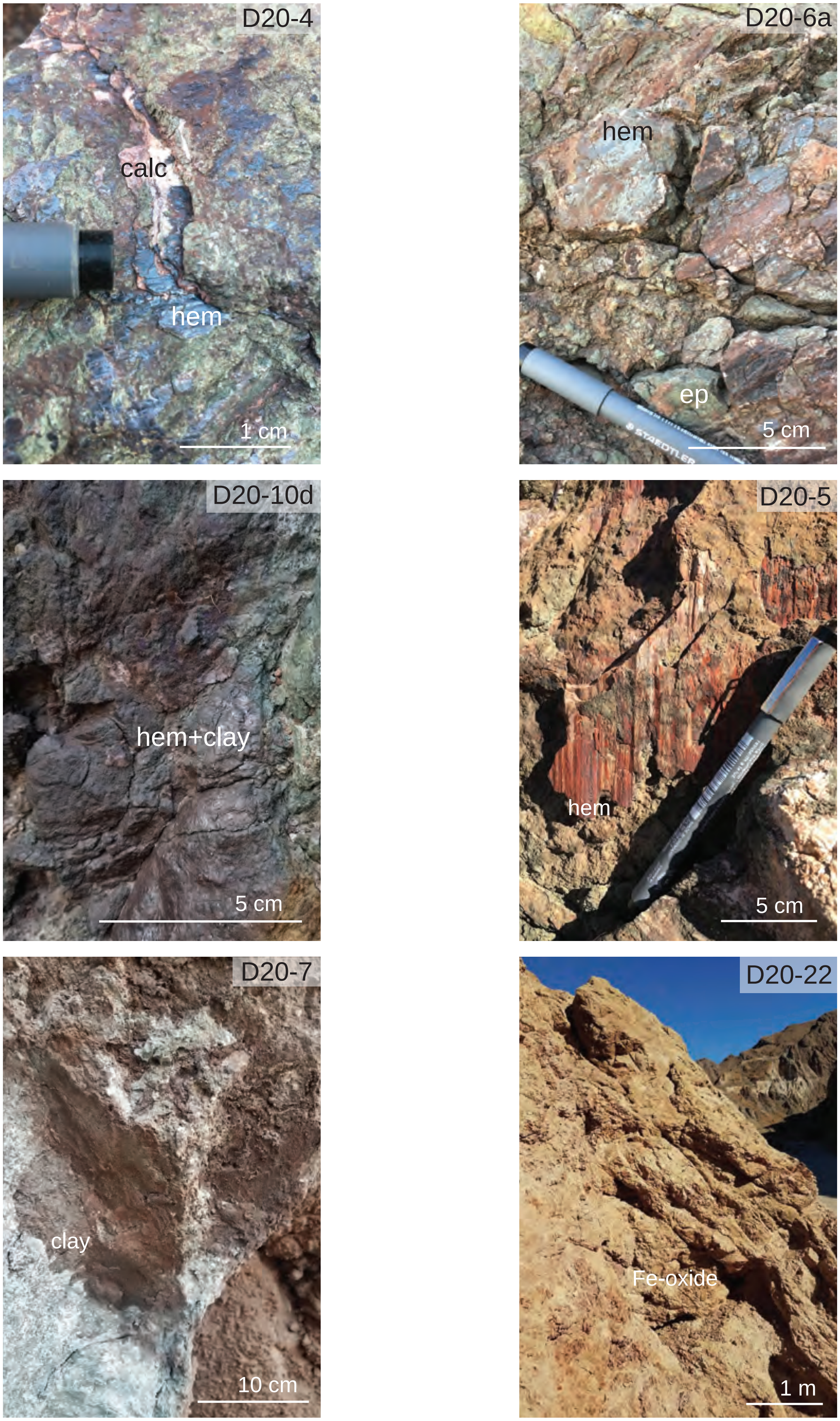

Figure S2. Field photographs of selected sample locations. calc = calcite, hem = hematite, ep = epidote.

Figure S3. Hand sample photographs. Circles identify target locations for aliquots for thermochronometry and microscopy.

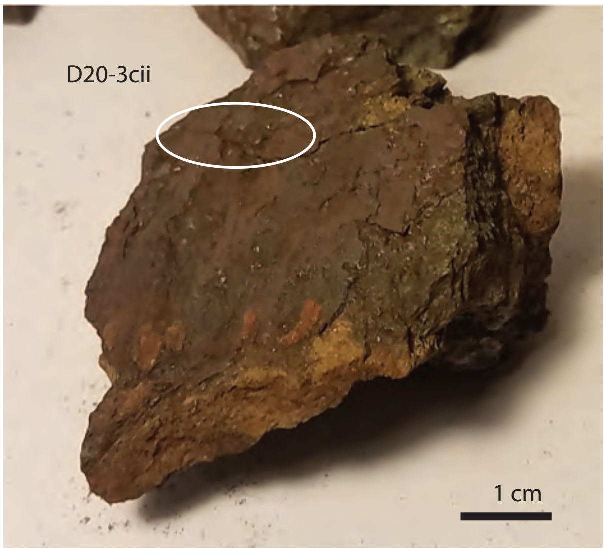

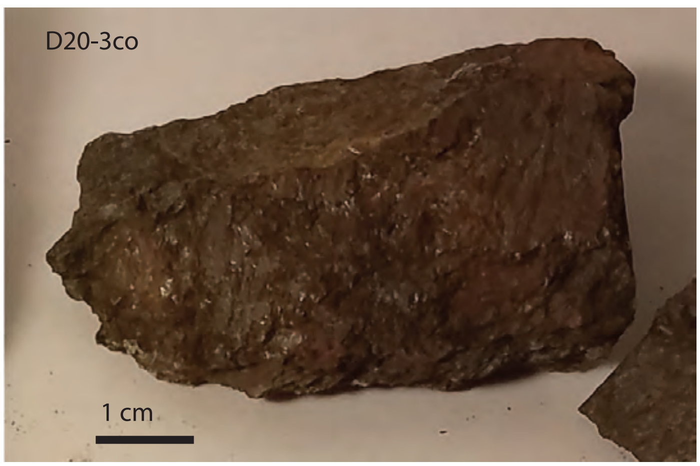

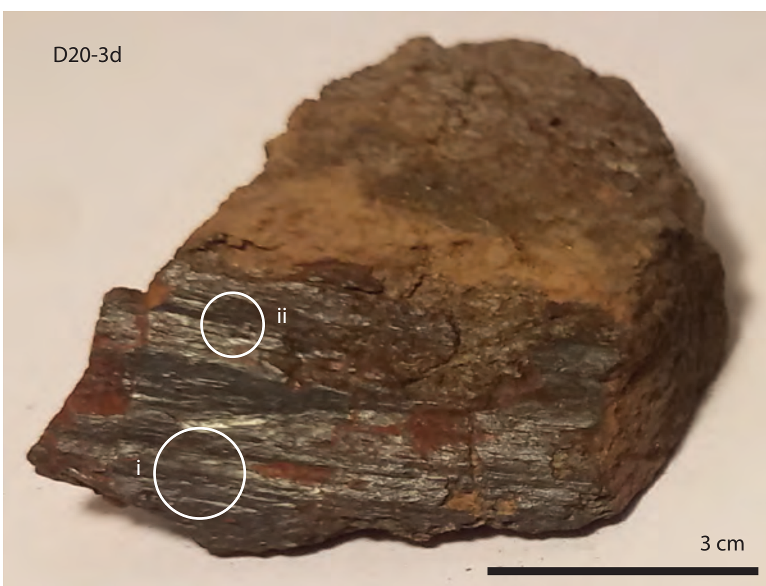

Figure S3 (continued).

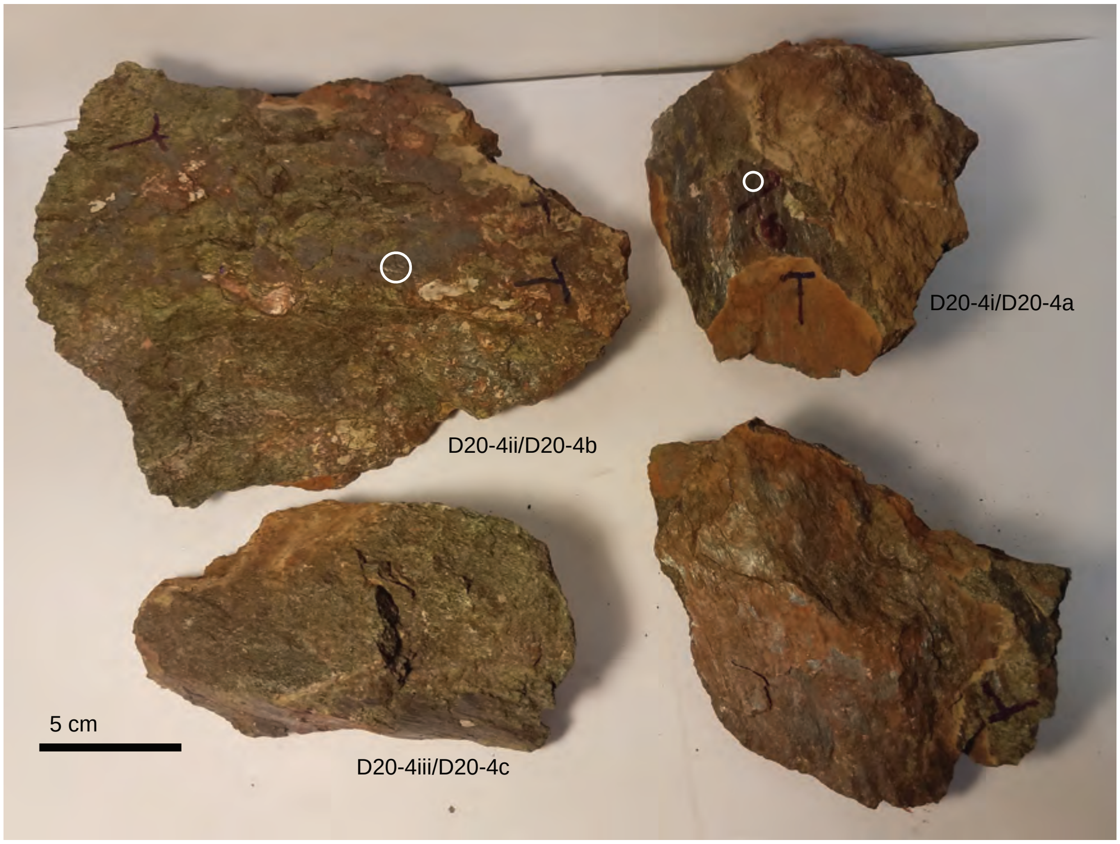

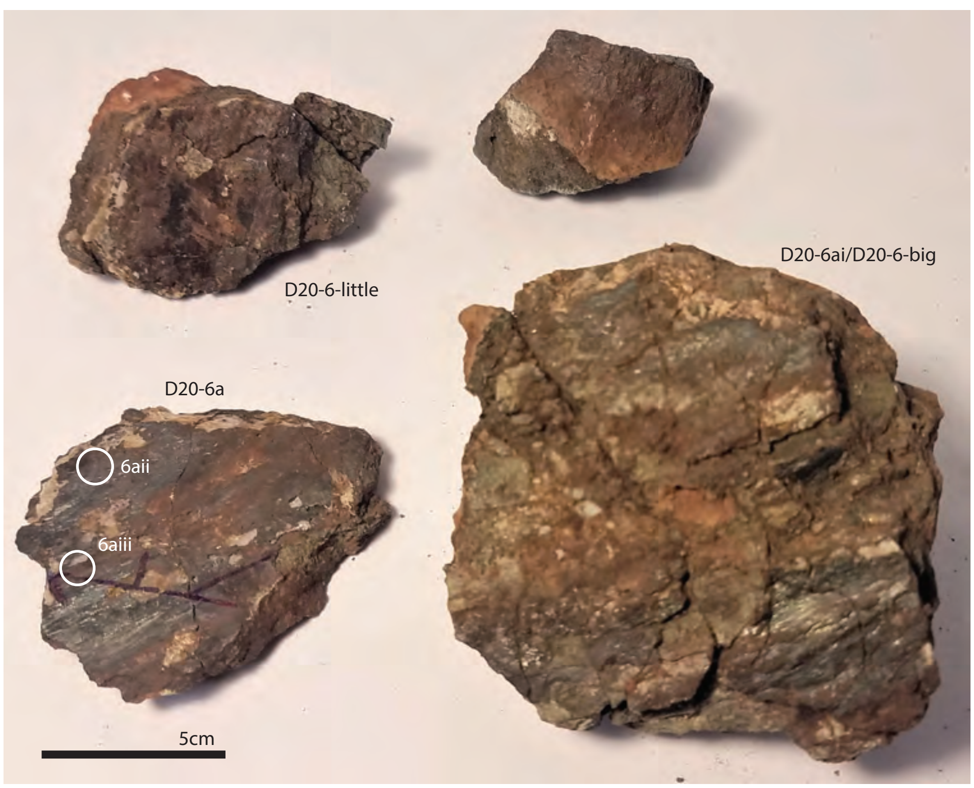

Figure S3 (continued).

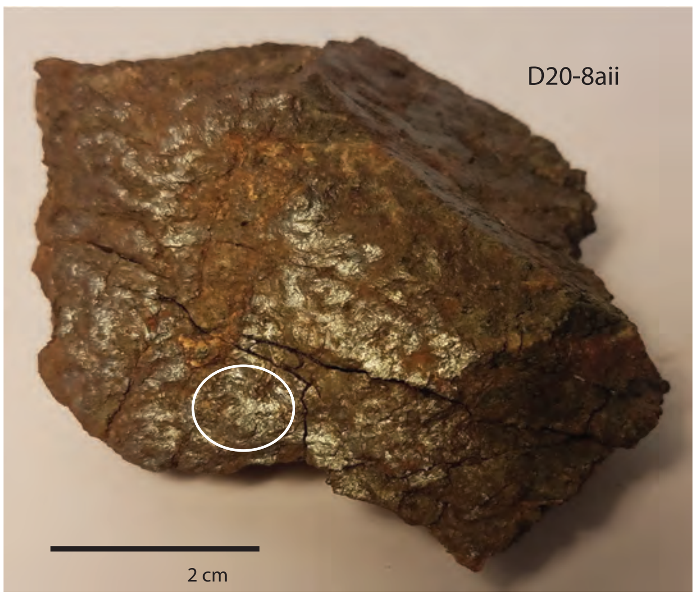

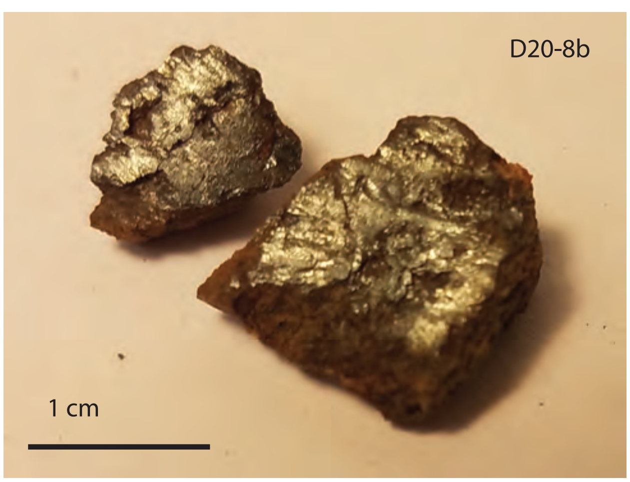

Figure S3 (continued).

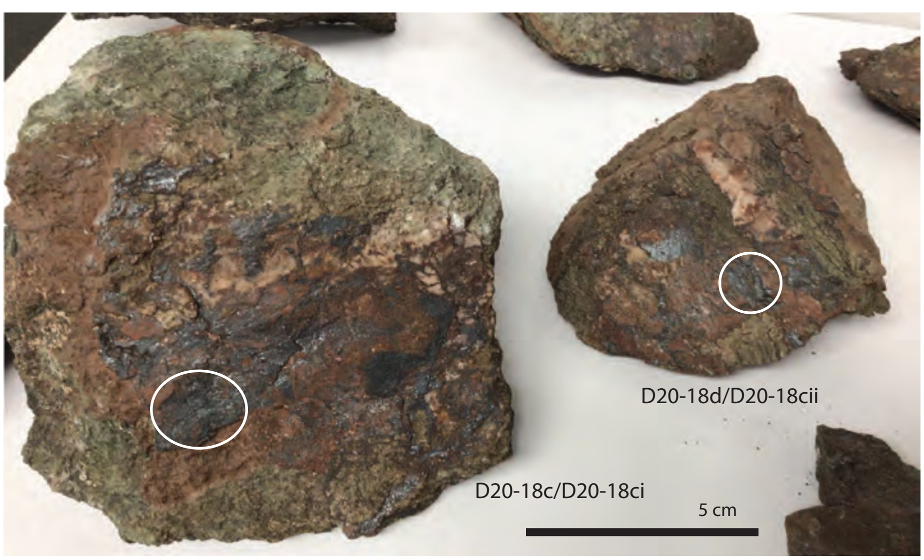

Figure S3 (continued).

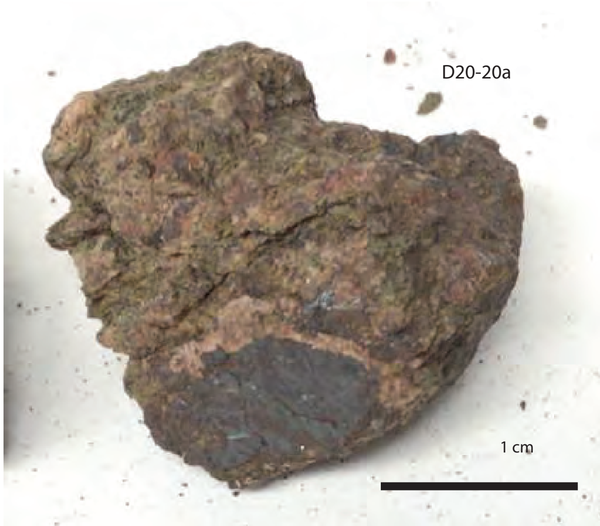

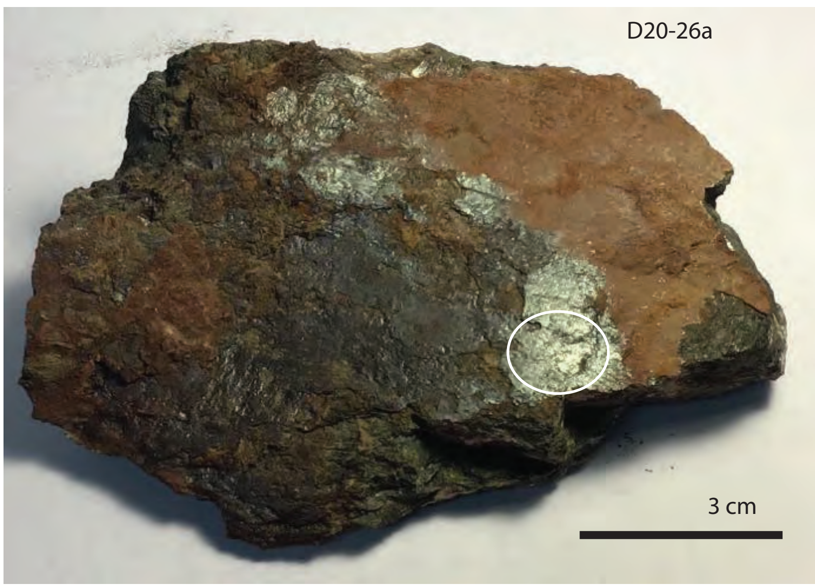

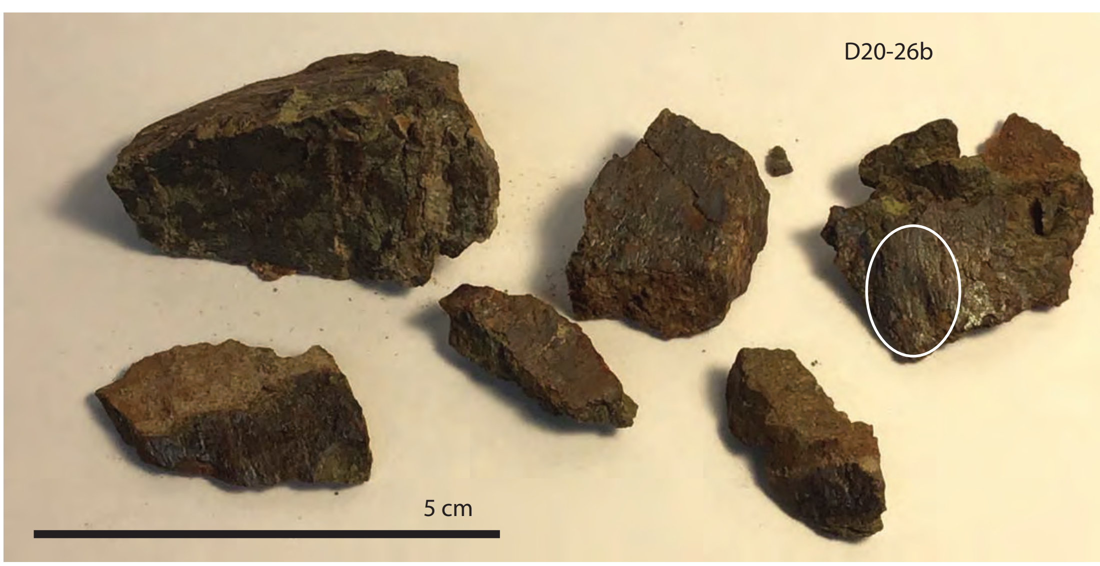

Figure S3 (continued).

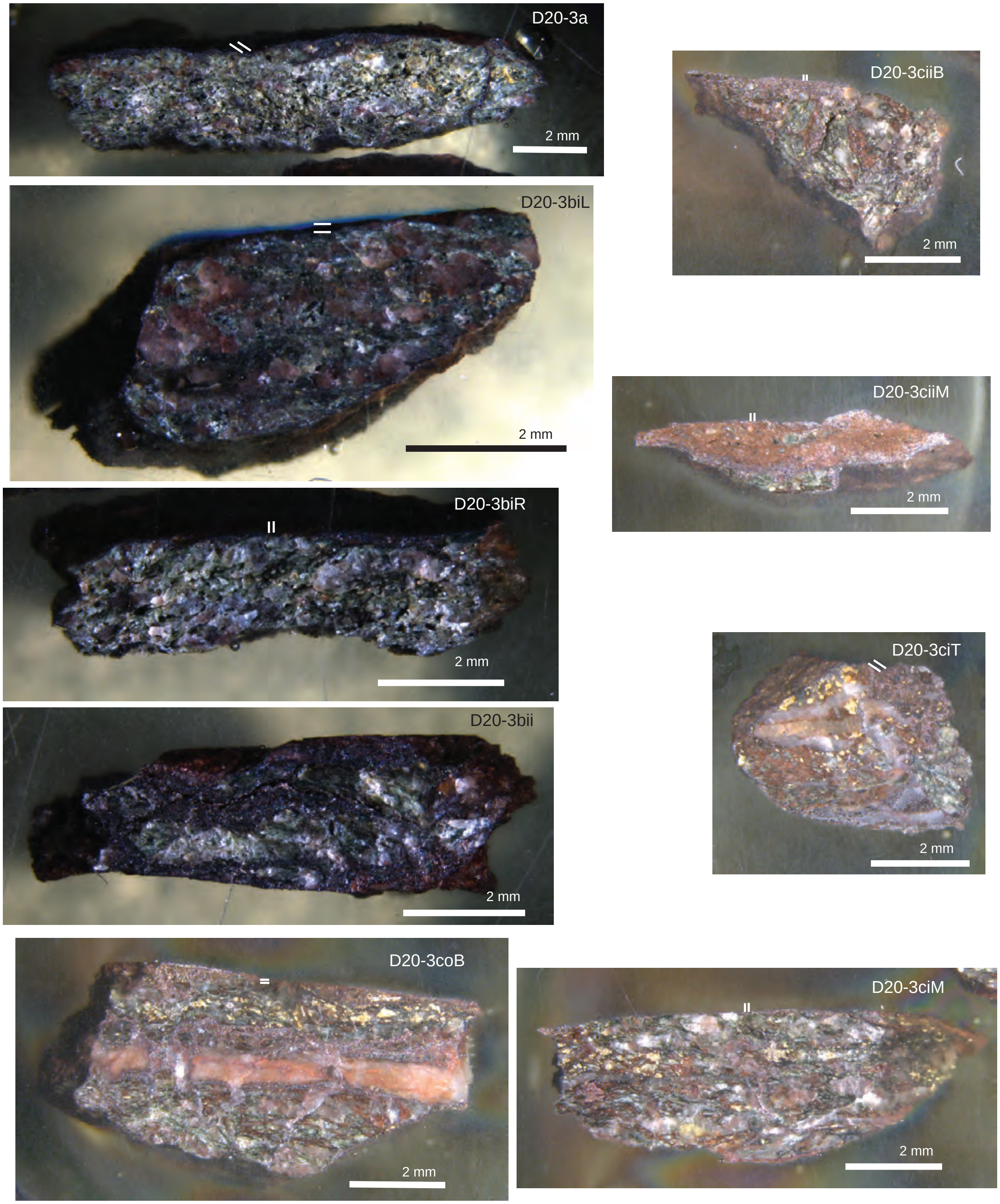

Figure S4. Photographs of sample chips in SEM epoxy mounts.

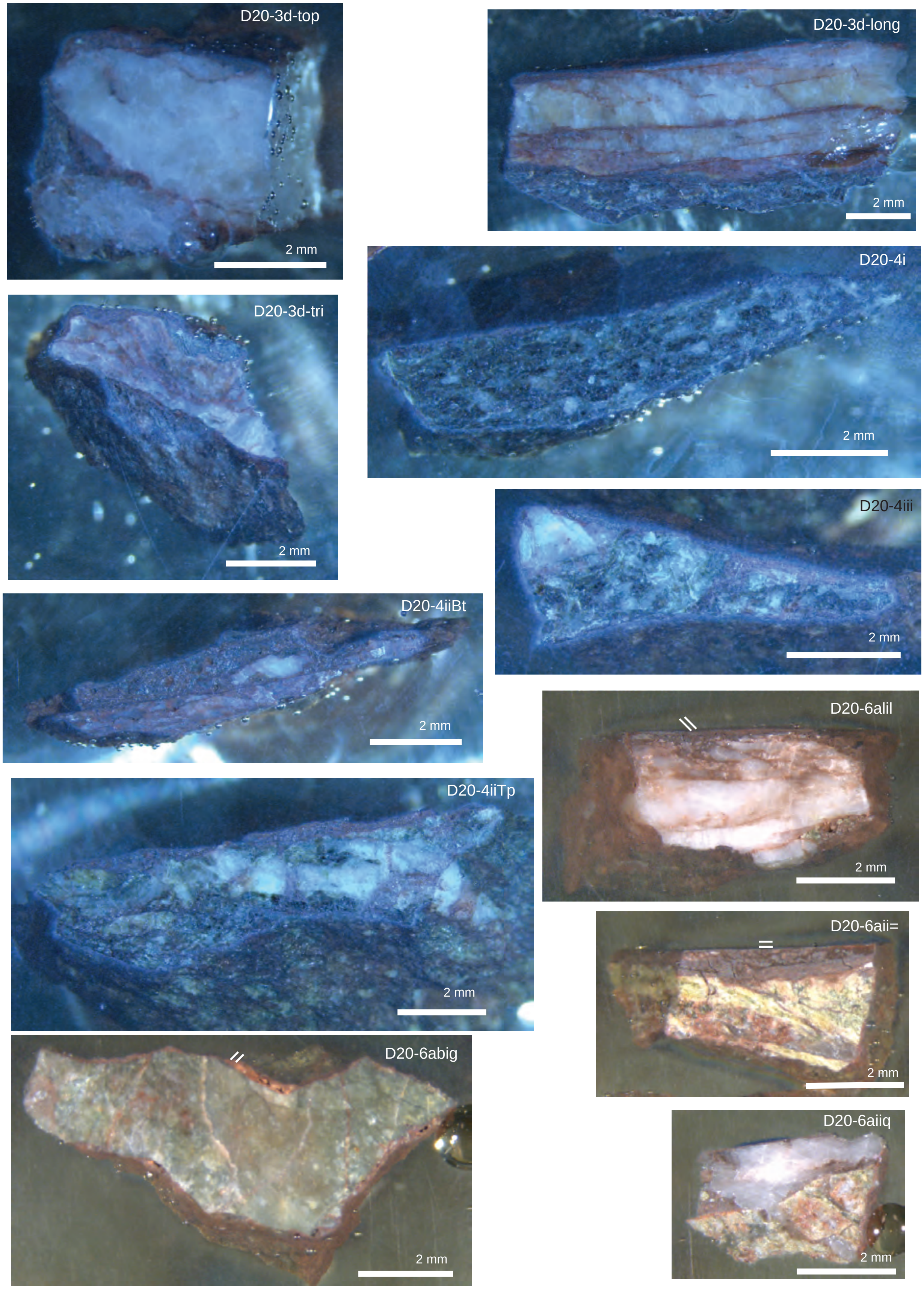

Figure S4 (continued)

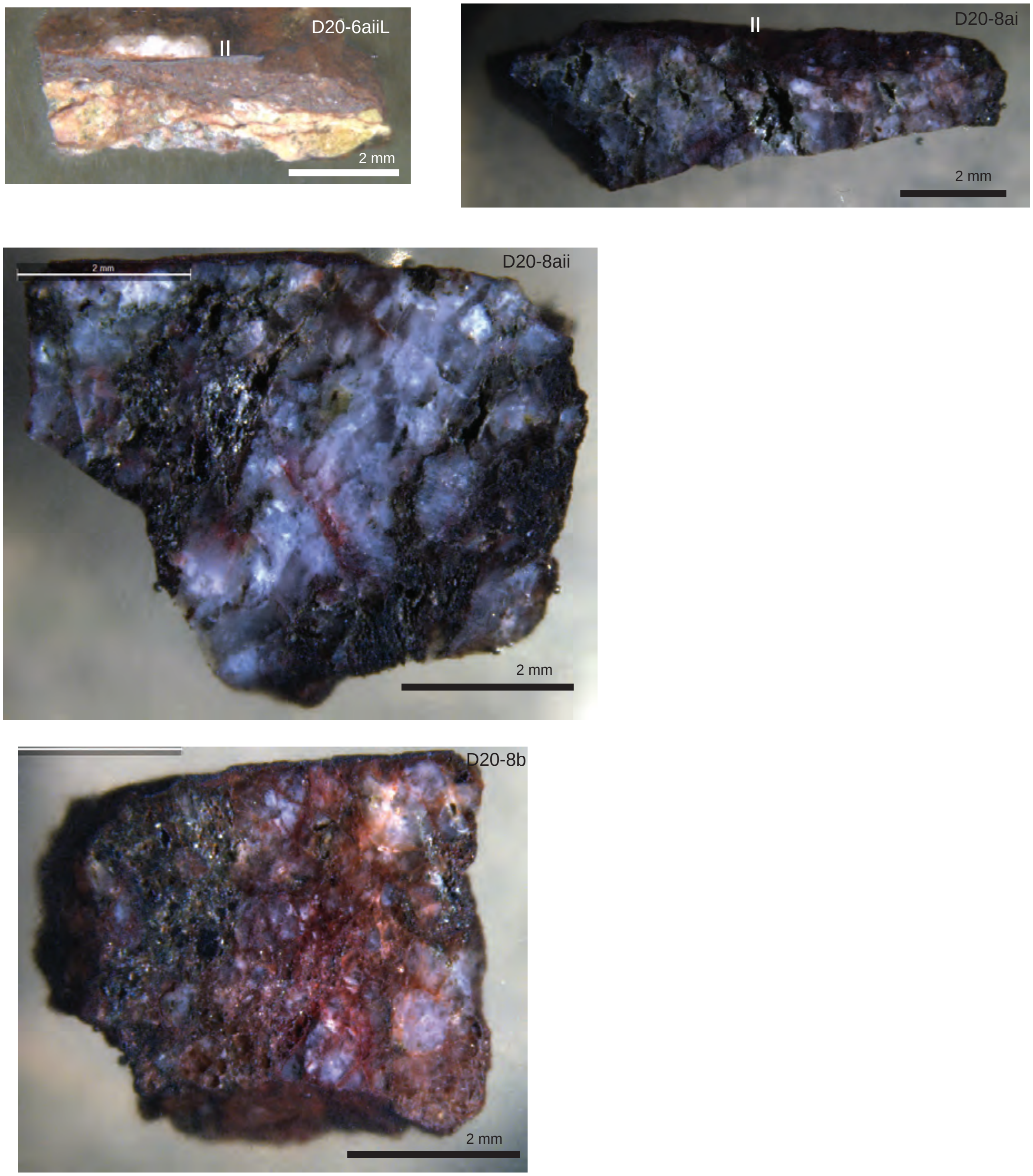

Figure S4 (continued).

Interlayered veins

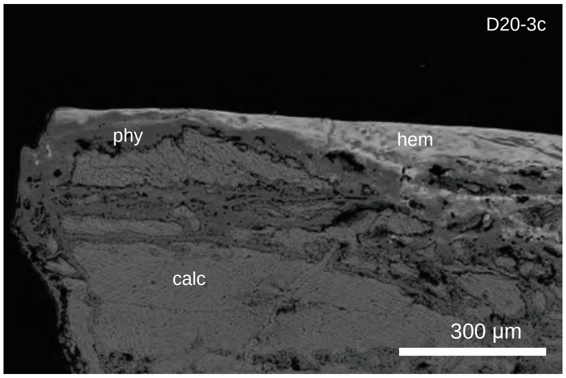

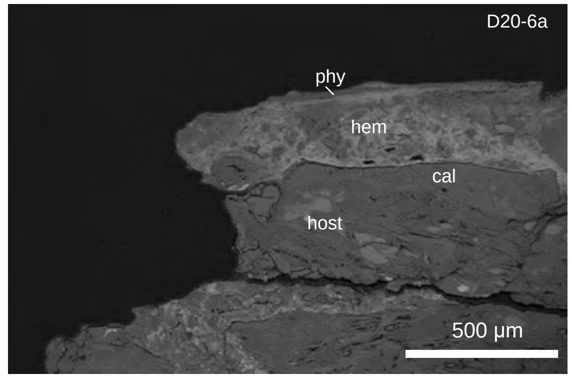

Other samples - 3b, 4a, 4b, 18c, 18d, 20a, 26a (main - 3d)

Hematite-filled injection veins

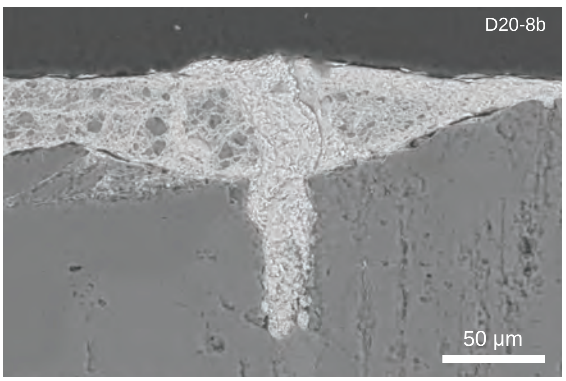

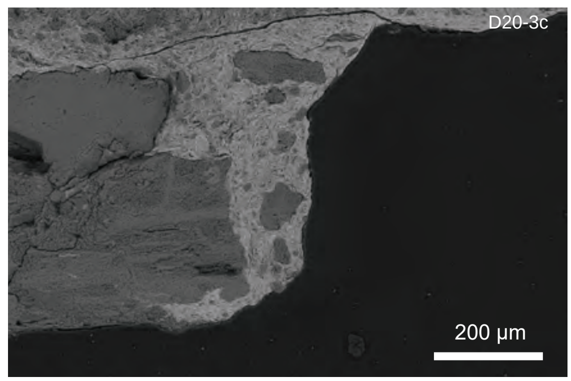

Other samples - 3b, 3d, 4a, 26a (main - 4b)

Reworked clasts and ‘hematite’ fish

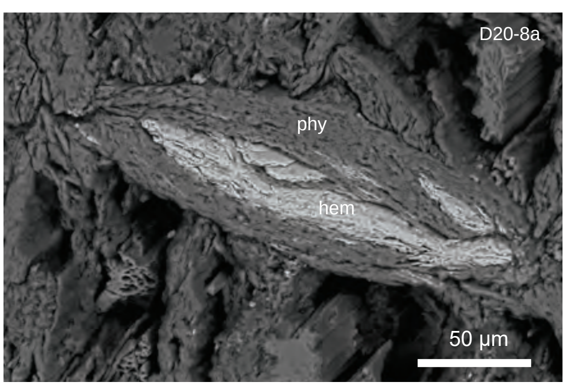

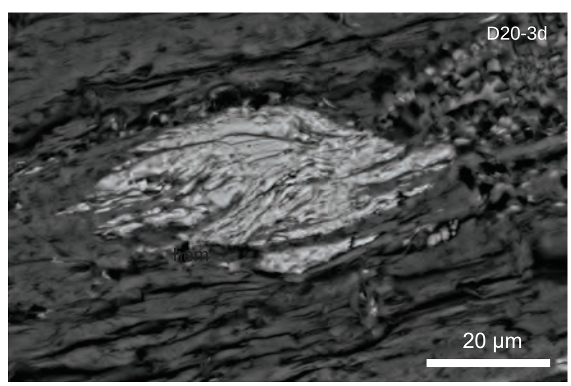

Other samples - 3b, 3c, 4a, 6a, 8a, 8b (main - 4b)

Figure S5. Additional SEM-BSE images of hematite microstructures. In addition to examples shown in images, other samples with each specific texture are noted.

Hematite tailed clasts and clast impressions

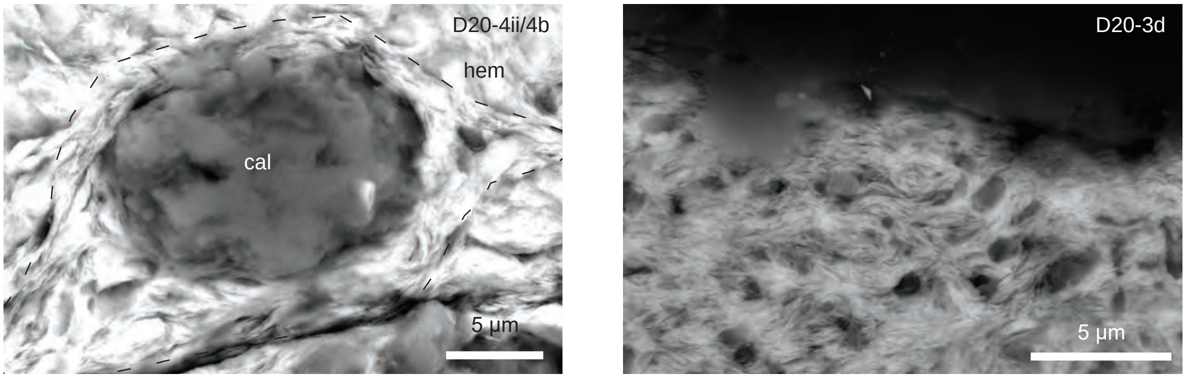

Other samples - 3a, 3b, 3c, 4a, 8a, 8b)

S-C fabrics developed in hematite

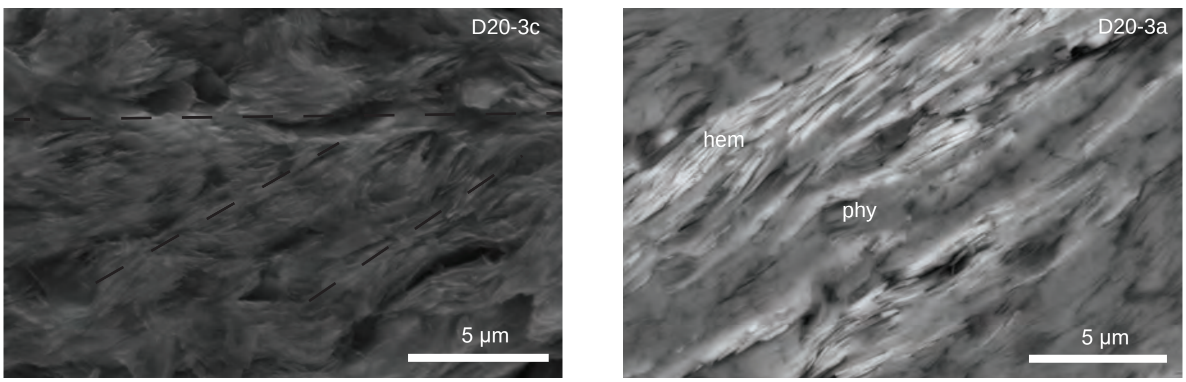

Other samples - 3d, 8a (main - 3b)

Clast-size sorted layers of hematite-matrix cataclasite

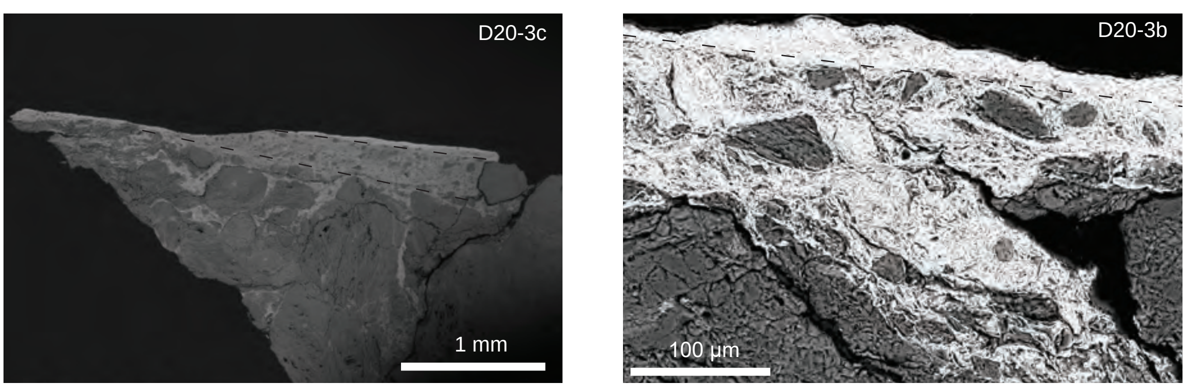

Other samples - 3a, 3d, 4a

Figure S5 (continued).

High aspect ratio plates

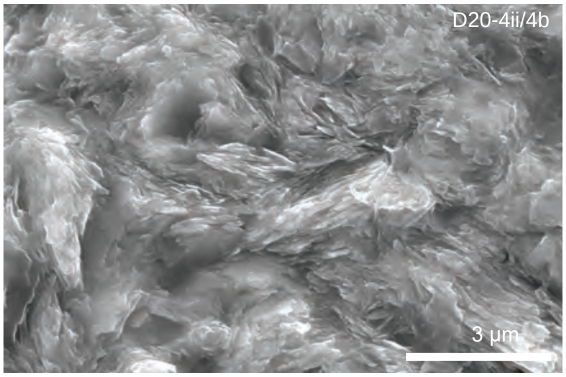

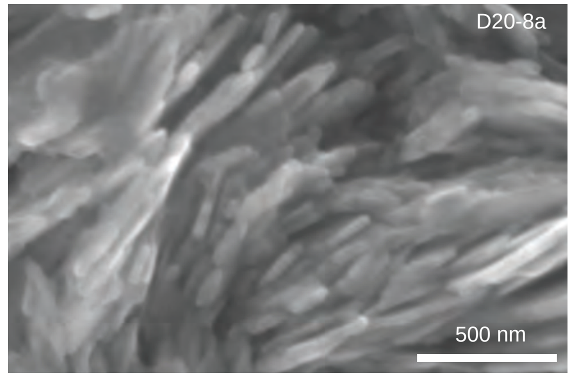

Other samples - 3b, 3c, 3d, 4a, 6a, 8b, 17g, 17h, 20a, 26a, 26b (main - 3a)

Plates with serrated grain boundaries

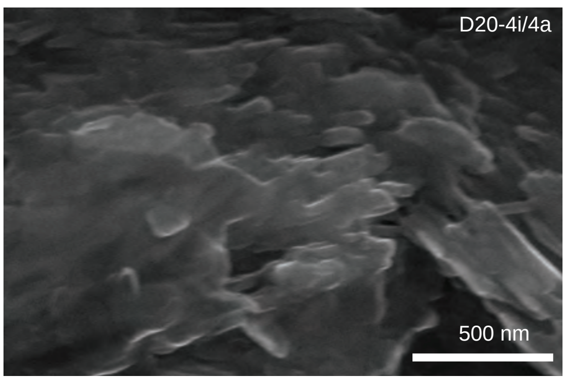

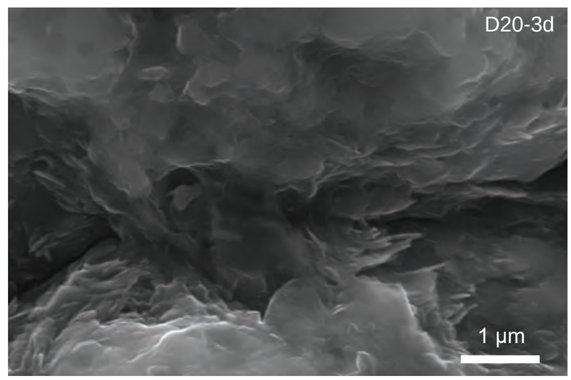

Other samples - 3a, 3b, 3c, 4b, 6a

Euhedral, hexagonal plates

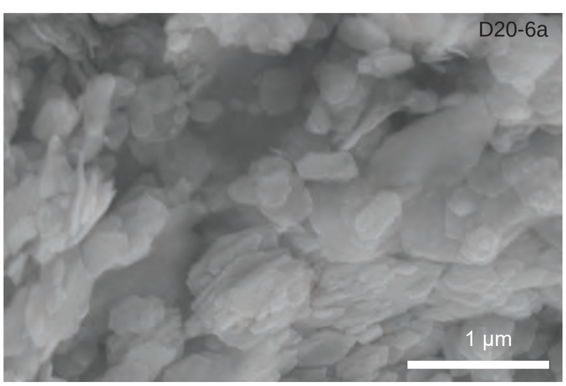

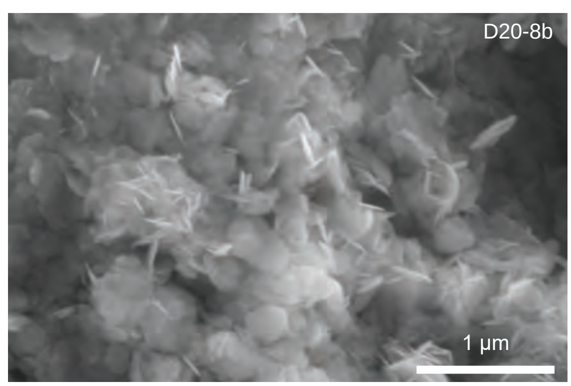

Other samples - 8a, 17g, 17h (main - 7)

Figure S6. Additional SEM-SE images of hematite morphologies. In addition to examples shown in images, other samples with each specific hematite grain morphologies are noted.

Stubby plates

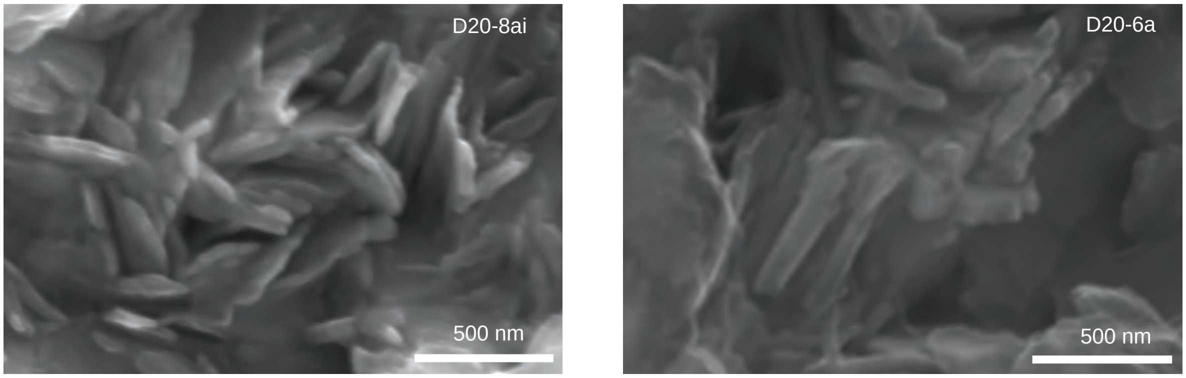

Other samples - 3c, 3d, 4a, 4b, 8aii 18c, 18d, 20a

‘Petal’-shaped plates

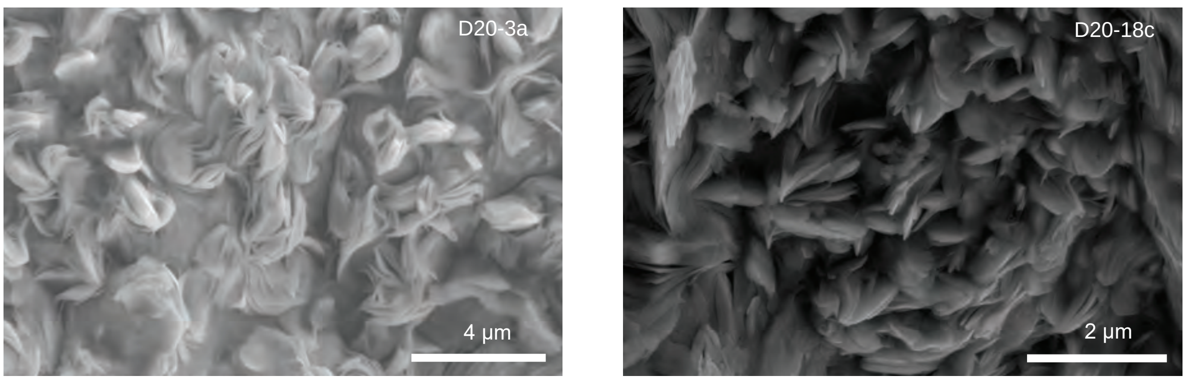

Other samples - 3b, 3c, 4a, 4b 8a, 8b, 17g, 17h, 18d, 20a, 26a, 26b

Figure S6 (continued).

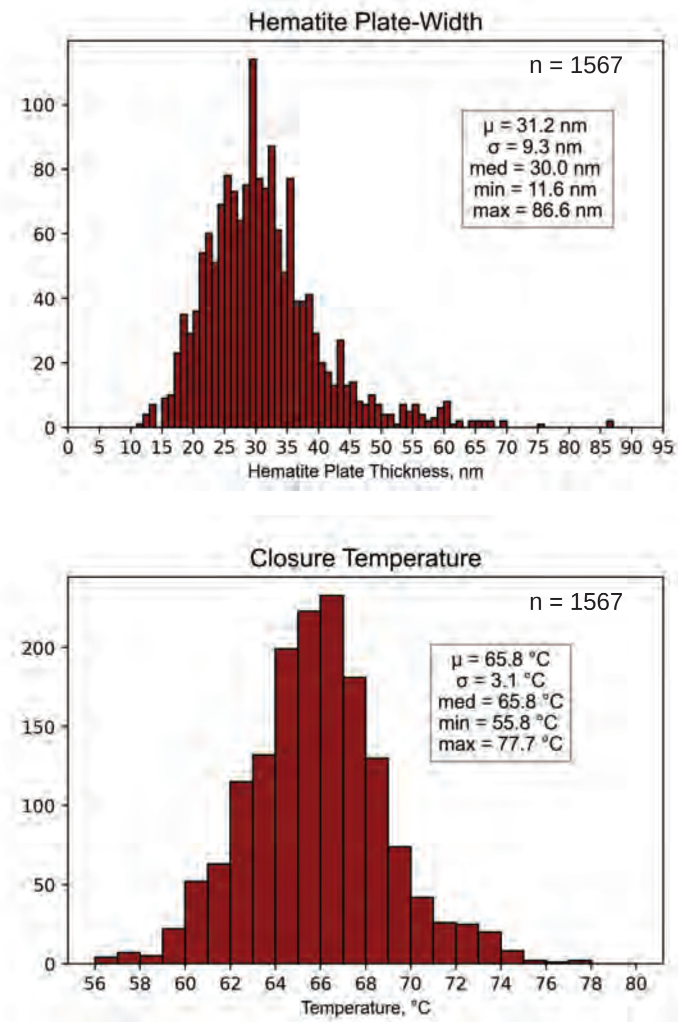

Figure S7. Histograms of hematite plate-width and calculated closure temperature (n = 1567 measurements). μ = mean, σ = standard deviation.

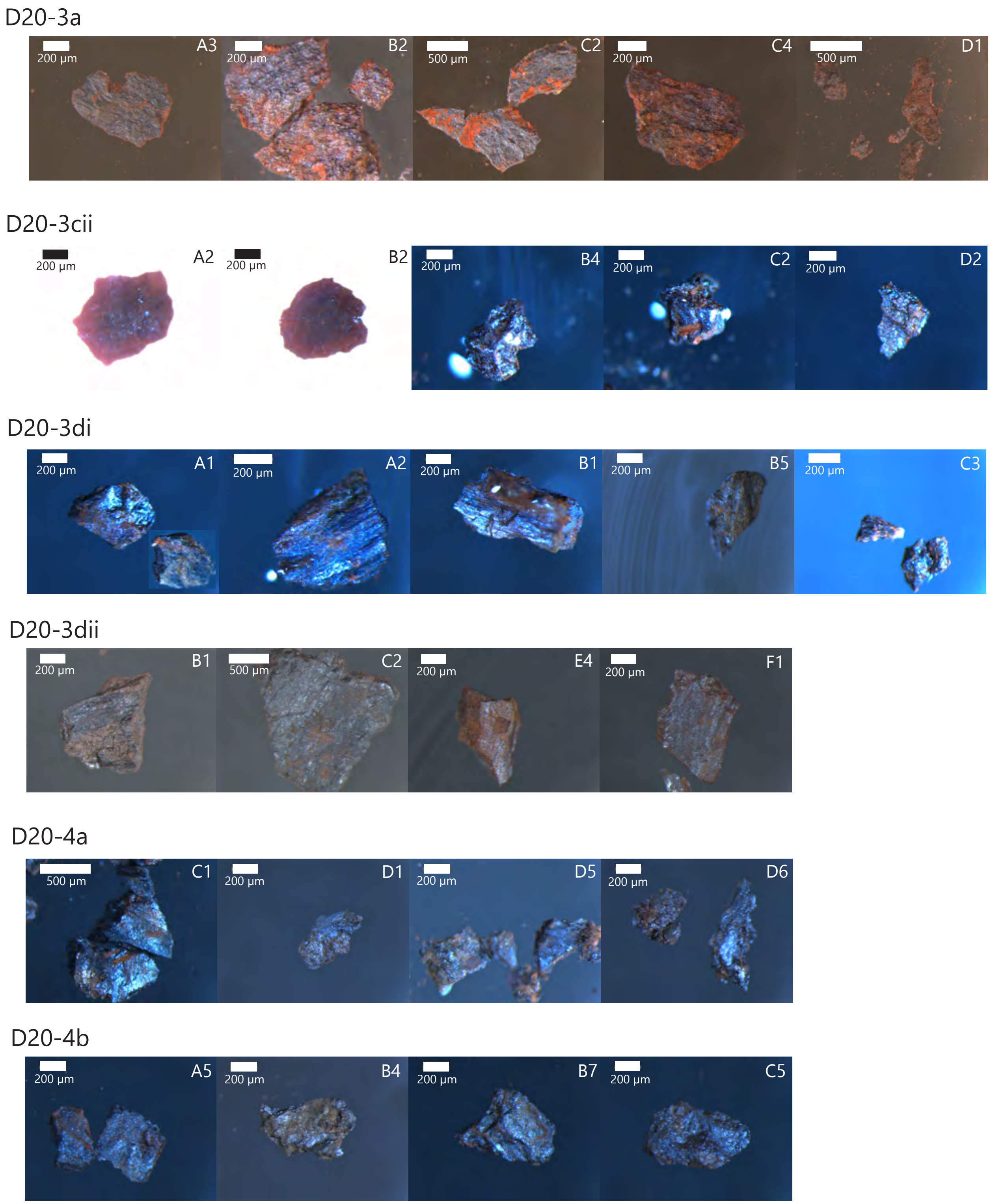

Figure S8. Stereoscopic photomicrographs of aliquots analyzed for (U-Th)/He thermochronometry.

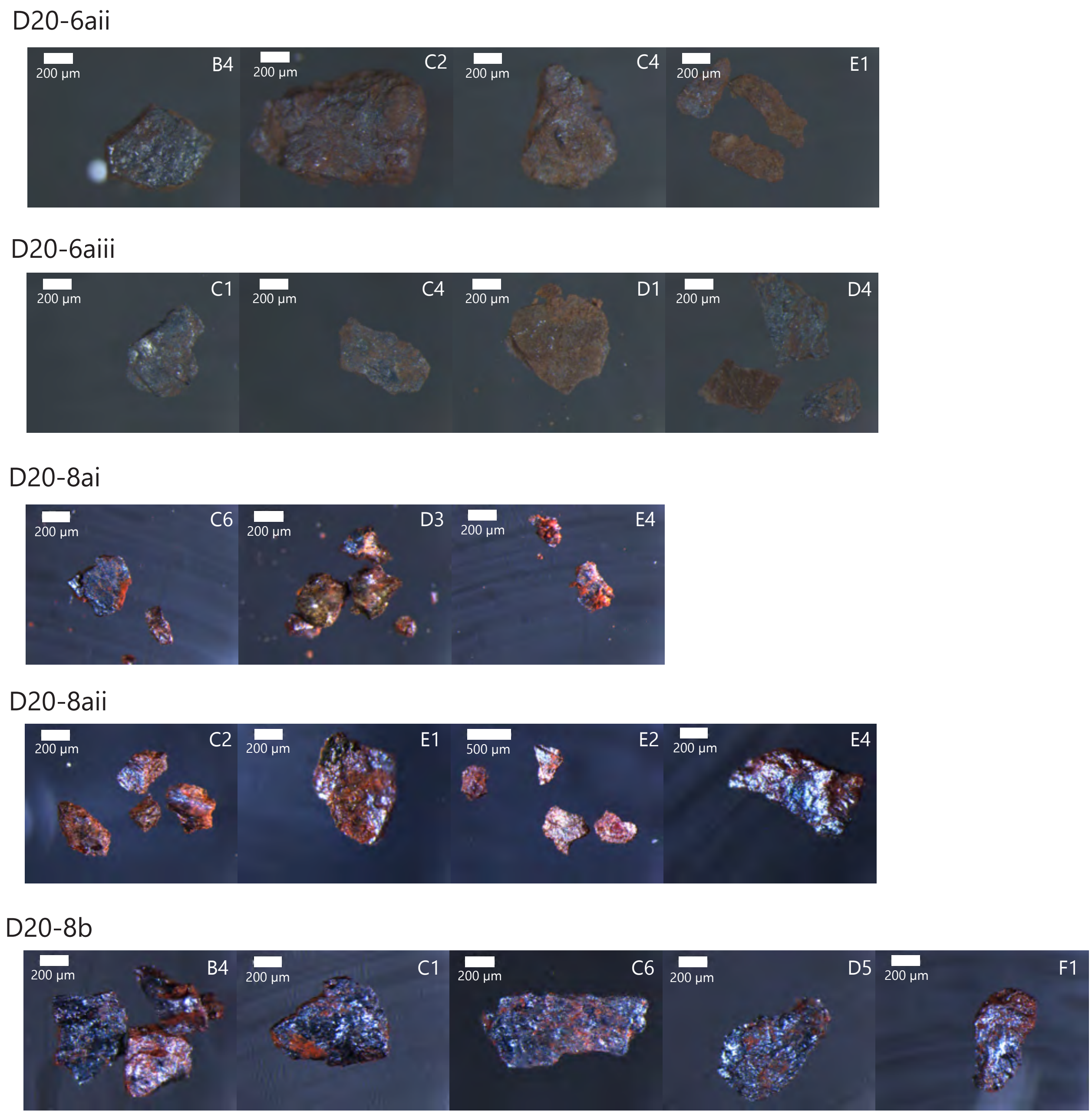

Figure S8 (continued).

D20-17g

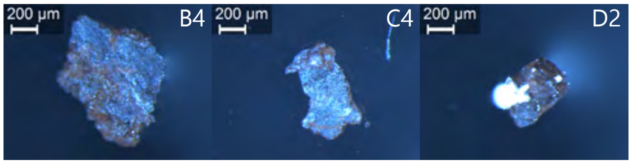

D20-17h

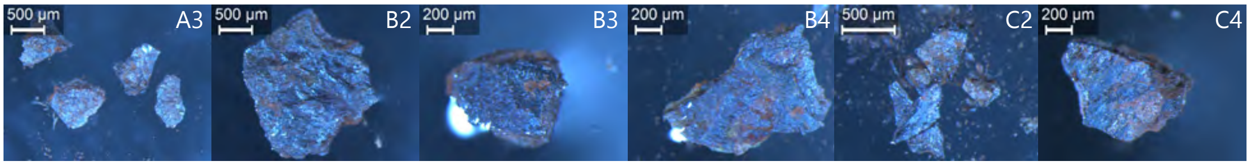

D20-18c

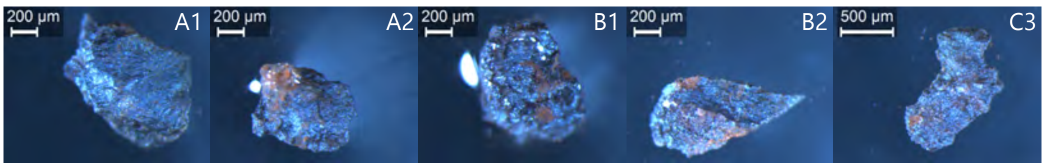

D20-18d

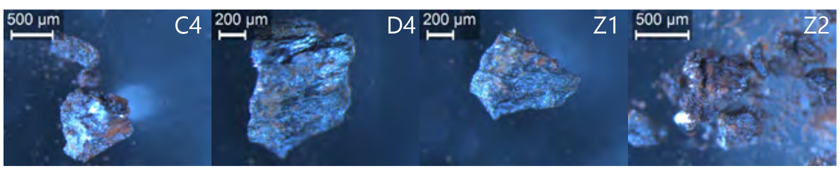

D20-20a

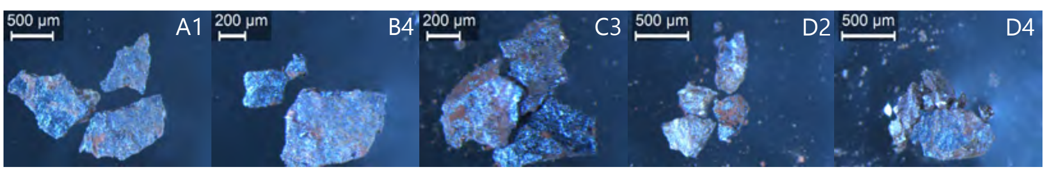

D20-26a

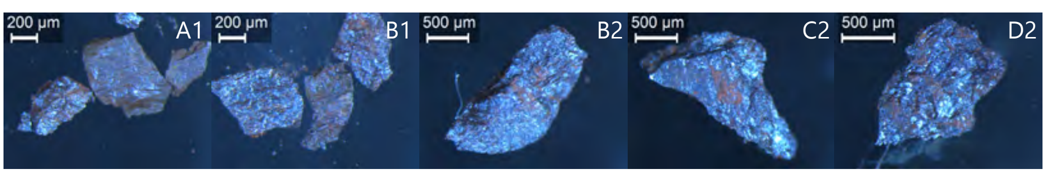

D20-26b

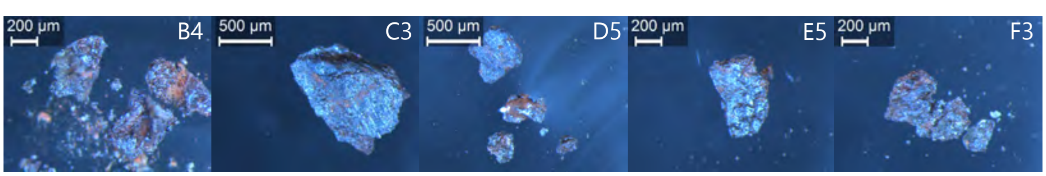

Figure S8 (continued).

```
In [1]: import numpy as np
```

```
In [2]: n = 10000000
        rat = 0.045                                        #insert th/u ratio
        hg = 75                                            #insert z height aliquot
        sdU = 13.605                                       #stopping dist hematite U238/U235 abundances
        sdTh = 16.04                                       #stopping dist hematite Th
        sd = (sdU*(1/(1+rat))) + (sdTh*(rat/(1+rat)))      #calculates average stopping distance
```

```
In [3]: #3-dimensional calculation

        threedth = np.random.random(n)* 360 + -180         #generates polar angle
        threedph = np.random.random(n)* 360 + -180         #generates azimuth angle
        radth = np.deg2rad(threedth)
        radph = np.deg2rad(threedph)
        x = np.random.random(n)                            #generates initial x pos
        y = np.random.random(n)                            #generates initial y pos
        z = np.random.random(n)* hg + -hg                  #generates initial z pos
        a = sd*np.cos(radph)*np.sin(radth)                 #x direction magnitude
        b = sd*np.sin(radph)*np.sin(radth)                 #y direction magnitude
        c = sd*np.cos(radth)                               #z direction magnitude
        s = (x+a, y+b, z+c)
        q = np.sqrt(a*a + b*b + c*c)
        sq = z+c                                           #z-direction new position

        vec = (sq > 0).sum()                               #loss in +z dir
        nvec = (sq < -hg).sum()                            #loss in -z dir if not balanced
        case = vec+nvec                                    #if both
        FT = 1-(vec/n)                                     #FT if one side balanced
        FTneither = 1-(case/n)                             #FT if He loss both sides

        print(FT)
        print(FTneither)

        0.9418202
        0.8836962
```

Figure S9. Python code implemented for F_T correction calculation (see text S3 for discussion).

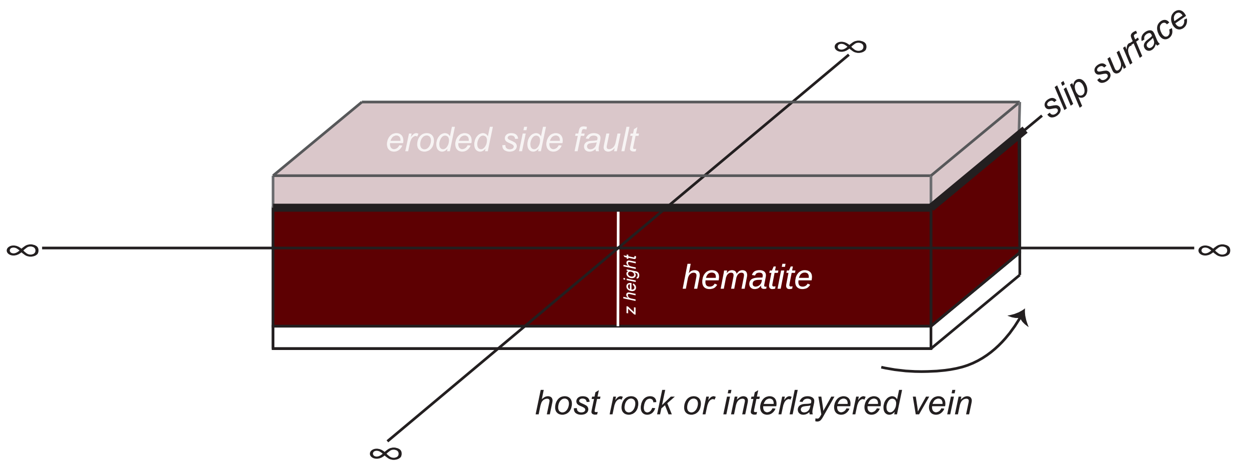

Figure S10. Schematic of hematite fault surface analyzed for (U-Th)/He thermochronometry demonstrating the parameters for the F_T correction (see text S3 for discussion).

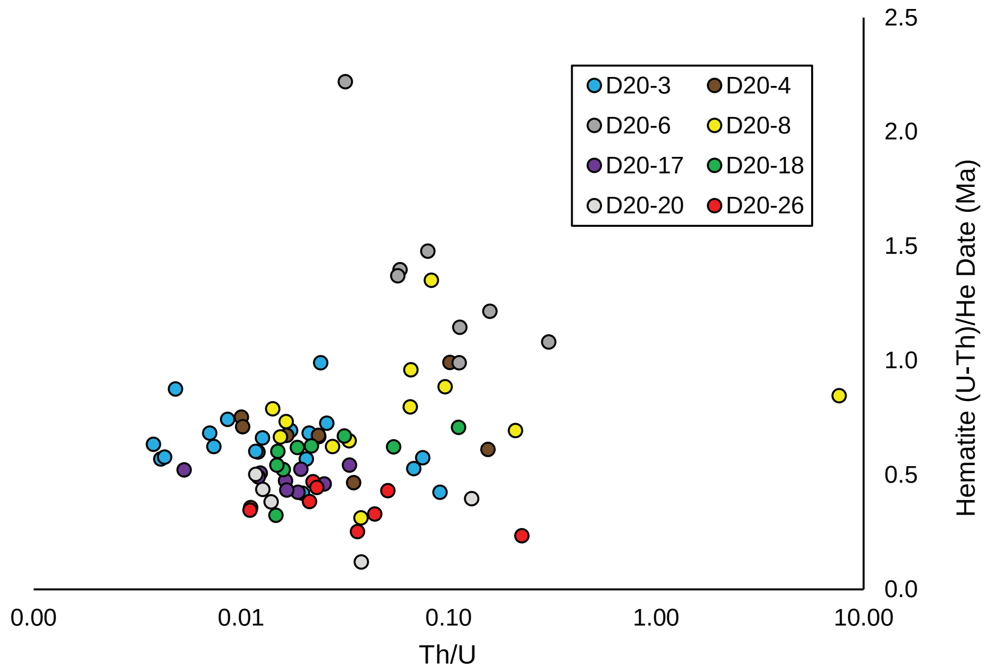

Figure S11. Individual hematite (U-Th)/He classified by sample as a function of Th/U to evaluate U loss during degassing (see text S2 for discussion).